

Beiträge aus der Automatisierungstechnik

**Chao Yao**

**A Contribution to the Design of Highly Redundant  
Compliant Aerial Manipulation Systems**

 VOGT

Dresden 2022

Bibliografische Information der Deutschen Nationalbibliothek  
Die Deutsche Nationalbibliothek verzeichnet diese Publikation in der  
Deutschen Nationalbibliografie; detaillierte bibliografische Daten sind im  
Internet über <http://dnb.dnb.de> abrufbar.

Bibliographic Information published by the Deutsche Nationalbibliothek  
The Deutsche Nationalbibliothek lists this publication in the Deutsche  
Nationalbibliografie; detailed bibliographic data are available on the Internet  
at <http://dnb.dnb.de>.

Zugl.: Dresden, Techn. Univ., Diss., 2022

Die vorliegende Arbeit stimmt mit dem Original der Dissertation  
„A Contribution to the Design of Highly Redundant Compliant Aerial  
Manipulation Systems“ von Chao Yao überein.

© Jörg Vogt Verlag 2022  
Alle Rechte vorbehalten. All rights reserved.

Gesetzt vom Autor

ISBN 978-3-95947-056-8

Jörg Vogt Verlag  
Niederwaldstr. 36  
01277 Dresden  
Germany

Phone: +49-(0)351-31403921  
Telefax: +49-(0)351-31403918  
e-mail: [info@vogtverlag.de](mailto:info@vogtverlag.de)  
Internet : [www.vogtverlag.de](http://www.vogtverlag.de)



**TECHNISCHE  
UNIVERSITÄT  
DRESDEN**

---

**Fakultät Elektrotechnik und Informationstechnik** Institut für Automatisierungstechnik

---

**Ein Beitrag zum Entwurf hochredunderter,  
nachgiebiger Luftmanipulationssysteme**

A Contribution to the Design of Highly Redundant  
Compliant Aerial Manipulation Systems

**Chao Yao**

von der Fakultät Elektrotechnik und Informationstechnik  
der Technischen Universität Dresden

zur Erlangung des akademischen Grades eines

**Doktoringenieurs**

(Dr.-Ing.)

genehmigte Dissertation

— \* —

Vorsitzender: Prof. Dr.-Ing. habil. Dipl.-Math. Klaus Röbenack

Gutachter: Prof. Dr. techn. Klaus Janschek  
Prof. Dr.-Ing. Walter Fichter

Tag der Einreichung: 26.11.2021

Tag der Verteidigung: 05.07.2022



## Danksagung

Carrying out the requisite work and then writing this thesis was undoubtedly the most arduous task I have undertaken. However, one of the joys of having completed the thesis is looking back at everyone who has helped me over the past three, six, and thirty-four years.

First of all, I would like to thank my supervisor, Prof. Klaus Janschek, the director of the Chair of Automation Technology, for his efforts over the years to secure adequate funding so that I could pursue my research interests without additional worries. This thesis would never have existed without his support. He has also given a great deal of helpful advice to improve the manuscript.

I would also like to acknowledge Prof. Walter Fichter from the Institute of Flight Mechanics and Control of the University of Stuttgart for accepting the role of co-referee of my doctorate thesis as well as his overall interest in my work.

My sincere gratitude also applies to Dr. Zhixing Zhao and Leon Stauder for their helpful advice on the manuscript.

Furthermore, I would like to extend my gratitude to my (former) colleagues at IfA and DMT, especially Dr. Martin Seemann, Dr. Frank Schnitze, Micha Schuster, David Bernstein, Bangshang Liu, Dr. Kai Ding, Lukas Baron, and Dr. Karim Bondoky, for an exceptionally supportive and friendly atmosphere with numerous fruitful discussions on a broad range of topics.

In addition, I am really grateful to my parents and my brother for their constant support and encouragement throughout my years of study up to the completion of this thesis.

Above all I deeply thank my wife Jing Xia for her wholehearted love, sympathetic ear, endless patience, and unwavering belief in me, for all the late nights and early mornings. It was her love that raised me up again when I got weary.



## Kurzfassung

Es ist vorhersehbar, dass die Luftmanipulatoren in den nächsten Jahrzehnten für viele Aufgaben eingesetzt werden, die entweder zu gefährlich oder zu teuer sind, um sie mit herkömmlichen Methoden zu bewältigen. In dieser Arbeit wird eine neuartige Lösung für die Gesamtsteuerung von hochredundanten Luftmanipulationssystemen vorgestellt. Die Ergebnisse werden auf eine Referenzkonfiguration angewendet, die als universelle Plattform für die Durchführung verschiedener Luftmanipulationsaufgaben etabliert wird. Diese Plattform besteht aus einer omnidirektionalen Drohne und einem seriellen Manipulator. Um den modularen Regelungsentwurf zu gewährleisten, werden zwei rechnerisch effiziente Algorithmen untersucht, um den virtuellen Eingang den Aktuatorbefehlen zuzuordnen. Durch die Integration eines auf einem künstlichen neuronalen Netz basierenden Diagnosemoduls und der rekonfigurierbaren Steuerungszuordnung in den Regelkreis, wird die Fehlertoleranz für die Drohne erzielt. Außerdem wird die Motorsättigung durch Rekonfiguration der Geschwindigkeits- und Beschleunigungsprofile behandelt. Für die Beobachtung der externen Kräfte und Drehmomente werden zwei Filter vorgestellt. Dies ist notwendig, um ein nachgiebiges Verhalten des Endeffektors durch die achsenselektive Impedanzregelung zu erreichen. Unter Ausnutzung der Redundanz des vorgestellten Luftmanipulators wird ein Regler entworfen, der nicht nur die Referenz der Endeffektor-Bewegung verfolgt, sondern auch priorisierte sekundäre Aufgaben ausführt. Die Wirksamkeit der vorgestellten Lösungen wird durch umfangreiche Tests überprüft, und das vorgestellte Steuerungssystem wird als sehr vielseitig und effektiv bewertet.







## Abstract

In the following decades, aerial manipulators are expected to be deployed in scenarios that are either too dangerous for human beings or too expensive to be accomplished by traditional methods. This thesis presents a novel solution for the overall control of highly redundant aerial manipulation systems. The results are applied to a reference configuration established as a universal platform for performing various aerial manipulation tasks. The platform consists of an omnidirectional multirotor UAV and a serial manipulator. To ensure modular control design, two computationally efficient algorithms are studied to allocate the virtual input to actuator commands. Fault tolerance of the aerial vehicle is achieved by integrating a diagnostic module based on an artificial neural network and the reconfigurable control allocation into the control loop. Besides, the risk of input saturation of individual rotors is minimized by predicting and reconfiguring the speed and acceleration responses. Two filter-based observers are presented to provide the knowledge of external forces and torques, which is necessary to achieve compliant behavior of the end-effector through an axis-selective impedance control in the outer loop. Exploiting the redundancy of the proposed aerial manipulator, the author has designed a control law to achieve the desired end-effector motion and execute secondary tasks in order of priority. The effectiveness of the proposed designs is verified with extensive tests generated by following Monte Carlo method, and the presented control scheme is proved to be versatile and effective.





# Inhaltsverzeichnis

<b>Kurzfassung</b>	<b>v</b>
<b>Abstract</b>	<b>vii</b>
<b>Inhaltsverzeichnis</b>	<b>ix</b>
<b>1 Introduction</b>	<b>1</b>
1.1 Motivation . . . . .	1
1.2 Research Objectives . . . . .	3
1.3 State of the Art . . . . .	4
1.3.1 Aerial Manipulation . . . . .	4
1.3.2 Fully Actuated UAVs . . . . .	7
1.3.3 Control Strategies of Multirotors . . . . .	9
1.3.4 Control Allocation . . . . .	12
1.3.5 UAV Fault-Tolerant Control . . . . .	14
1.3.6 Input Constraint Considerations . . . . .	17
1.3.7 Wrench Observer . . . . .	17
1.4 Scientific Contributions . . . . .	18
1.5 Thesis Structure . . . . .	23
<b>2 Fundamentals</b>	<b>25</b>
2.1 3D Rigid Transformations . . . . .	25
2.2 Orientation Representation . . . . .	27
2.2.1 Euler Angles . . . . .	27
2.2.2 Axis-Angle Parameterization . . . . .	28
2.2.3 Quaternions . . . . .	29
2.3 Moore-Penrose Inverse . . . . .	29
2.4 Ridders' Method . . . . .	30
2.5 Null Space . . . . .	32
2.6 Long Short-Term Memory . . . . .	32
<b>3 System Design and Modeling</b>	<b>35</b>
3.1 Design and Modeling of the Multirotor UAV . . . . .	35
3.1.1 Tilt-Hexarotor Design . . . . .	35

3.1.2	Kinematics . . . . .	37
3.1.3	Dynamics . . . . .	40
3.1.4	Motor Modeling . . . . .	42
3.2	Design and Modeling of the Serial Manipulator . . . . .	42
3.2.1	Manipulator Design . . . . .	42
3.2.2	Forward Kinematics . . . . .	45
3.2.3	Differential Kinematics . . . . .	48
3.3	Dynamics of the Whole Aerial Manipulator . . . . .	52
<b>4</b>	<b>Reconfigurable Control Allocation</b>	<b>57</b>
4.1	Extended Thrust Formulation . . . . .	57
4.2	Cascading Moore-Penrose Inverse . . . . .	58
4.3	IPM-Based Quadratic Programming . . . . .	60
4.4	Emergency Routine . . . . .	63
4.5	Reconfiguration for Rotor Faults . . . . .	64
4.6	Performance Comparison . . . . .	65
<b>5</b>	<b>Fault Diagnostics For Free Flight</b>	<b>75</b>
5.1	LSTM-Based FDI . . . . .	75
5.2	LSTM-Based Fault Estimation . . . . .	78
5.3	Simulation and Performance Comparison . . . . .	79
5.3.1	Detection and Isolation of Single Fault . . . . .	79
5.3.2	Detection and Isolation of Two Faults . . . . .	83
5.3.3	Estimation of Partial Fault . . . . .	84
<b>6</b>	<b>Force and Torque Observer</b>	<b>87</b>
6.1	State-Space Representation . . . . .	88
6.1.1	Nonlinear Model for EKF . . . . .	88
6.1.2	Linear Model for KF . . . . .	90
6.2	Observability Analysis . . . . .	91
6.3	Algorithm Structure . . . . .	95
6.4	Consistency Test . . . . .	97
6.5	Timing Statistics . . . . .	100
6.6	Performance Analysis with Case Study . . . . .	101
<b>7</b>	<b>Trajectory Generation</b>	<b>113</b>
7.1	Interpolation in SE(3) . . . . .	113
7.2	Saturation-free Trajectory generator for Free Flight . . . . .	114
7.2.1	Rotor Constraints . . . . .	114

7.2.2	Prediction and Reconfiguration of Rotor Speed . . . .	115
7.2.3	Prediction and Reconfiguration of Rotor Acceleration	120
7.2.4	Workflow . . . . .	122
7.2.5	Test Results . . . . .	124
<b>8</b>	<b>Hybrid Task Priority Control</b>	<b>127</b>
8.1	Differential Flatness . . . . .	127
8.2	Pose Control with Exact Linearization . . . . .	129
8.3	Task Priority Control . . . . .	132
8.3.1	Inverse Differential Kinematics . . . . .	132
8.3.2	Secondary Tasks . . . . .	134
8.4	Axis-Selective Impedance Filter . . . . .	139
8.5	Test and Verification . . . . .	142
8.5.1	Impedance Filter . . . . .	143
8.5.2	Pose Control . . . . .	144
8.5.3	Secondary Tasks . . . . .	148
<b>9</b>	<b>System Integration and Performance Evaluation</b>	<b>157</b>
9.1	Fault-Tolerant Control for Free Flight . . . . .	157
9.1.1	Fault-Tolerant Control Scheme . . . . .	157
9.1.2	Results of FTC Test . . . . .	160
9.2	Evaluation of Hybrid Task Priority Control . . . . .	163
<b>10</b>	<b>Conclusion</b>	<b>169</b>
10.1	Summary . . . . .	169
10.2	Future Work . . . . .	172
<b>Anhang A</b>	<b>Generalized Inertia Tensor</b>	<b>177</b>
<b>Anhang B</b>	<b>Model Parameters</b>	<b>181</b>
B.1	Parameters of the UAV . . . . .	181
B.2	Denavit–Hartenberg Parameters of the Manipulator . . . . .	181
B.3	COM Location of the Links . . . . .	183
B.4	Mass of the Bodies . . . . .	183
B.5	Inertia Matrices of the Bodies . . . . .	184
<b>Anhang C</b>	<b>EKF-Based FDI</b>	<b>185</b>
<b>Anhang D</b>	<b>Case Study Results</b>	<b>189</b>



## Abbildungsverzeichnis

1.1	Examples of potential application scenarios for aerial manipulation. . . . .	2
1.2	Examples of two solutions for aerial manipulation. . . . .	4
1.3	Examples of manipulator configuration. . . . .	5
1.4	Examples of manipulator design. . . . .	6
1.5	Examples of Fully actuated UAVs with tilted rotors. . . . .	8
1.6	Examples of fully actuated UAVs with unconventional geometric structures. . . . .	9
1.7	Control system structure using control allocation. . . . .	12
1.8	Overview of the contributions and benefits. . . . .	19
1.9	Architecture of the proposed active fault-tolerant control. . . . .	21
2.1	Representation of the relation between the Lie group and the Lie algebra. . . . .	25
2.2	Yaw-pitch-roll ( $\psi$ - $\vartheta$ - $\varphi$ ) Euler sequence . . . . .	28
2.3	Basic concept of an artificial neural network. . . . .	33
2.4	Structure of a LSTM network. . . . .	33
3.1	Definition of the inertial frame $\{I\}$ , body frame $\{B\}$ , rotor frame $\{R_i\}$ and tilting angle $\alpha_i$ . . . . .	37
3.2	Force and torque capabilities and hover efficiency of the designed tilt-hexarotor expressed in $\{B\}$ . . . . .	38
3.3	Design methodology for a general robot manipulator. . . . .	43
3.4	Rendered view of the arm system. . . . .	44
3.5	Overall dimensions of the aerial manipulator with gripper in different configurations. . . . .	46
3.6	Rendered 3D view of the tools . . . . .	46
3.7	Definition of the coordinates frames of the manipulator system. . . . .	47
3.8	Workspace of the manipulator without tools shown in the frame $\{B\}$ . . . . .	49
3.9	Absolute values of the determinant of the sub-matrix $\mathbf{J}_{11}$ with respect to joint 2 and 3. . . . .	52
3.10	Definition of the coordinates frames of the whole system. . . . .	53

4.1	Three-dimensional demonstration of the emergency routines.	64
4.2	Tracking error of the CMPI using down-scaling and dimension reduction as emergency routines.	68
4.3	Hovering rotor speed of CMPI and IPM with rotor 1 and 4 deactivated one after the other.	70
4.4	Allocation Error of the CMPI algorithm with rotor 1 and 4 deactivated one after the other.	70
4.5	Allocation Error of the IPM algorithm with rotor 1 and 4 deactivated one after the other.	71
4.6	Schematic representation of the reference motion in closed-loop test.	71
4.7	Rotor speed of CMPI and IPM in closed-loop test.	72
4.8	Allocation Error of the CMPI algorithm in closed-loop test.	73
4.9	Allocation Error of the IPM algorithm in closed-loop test.	73
5.1	Preparation data for LSTM.	76
5.2	Architecture of the LSTM-based FDI.	76
5.3	Training process of a LSTM network.	77
5.4	Methodology of fault estimation.	78
5.5	Architecture of the LSTM model for fault estimation.	79
5.6	Randomly selected failure locations and time for single-fault tests.	80
5.7	Diagnostic results of 200 random simulations using the EKF-based FDI.	81
5.8	Diagnostic results of 200 random simulations using the LSTM-based FDI with $l_{LSTM} = 4$ .	81
5.9	Diagnostic results of 200 random simulations using the LSTM-based FDI with $l_{LSTM} = 7$ .	82
5.10	Diagnostic results of 200 random simulations using the LSTM-based FDI with $l_{LSTM} = 10$ .	82
5.11	Randomly selected failure locations and time for two-fault tests.	83
5.12	Diagnostic results of FDI for two faults.	84
5.13	Randomly selected failure locations, magnitudes and time for partial-fault tests.	85
5.14	Diagnostic results of fault estimation.	86
6.1	Architecture of a Kalman filter.	87
6.2	Average normalized estimation error squared.	99



6.3	Timing statistics of 10,000 loops for the observers. . . . .	100
6.4	Timing statistics of 100 loops for the EKF-based wrench observer with online/offline linearization. . . . .	101
6.5	Main structure of the simulation for case study. . . . .	102
6.6	Reference and estimated wrench of the EKF and the KF in Test A.1. . . . .	104
6.7	Estimation errors of the EKF and the KF in Test A.1. . . . .	105
6.8	Selected estimation errors of the EKF and the KF in Test B.1. . . . .	106
6.9	Selected estimation errors of the EKF and the KF in Test C.1. . . . .	106
6.10	Reference and estimated forces of the EKF and the KF in Test D.1. . . . .	107
6.11	Selected estimation errors of the EKF and the KF in Test D.1. . . . .	108
6.12	Reference and estimated torques of the EKF and the KF in Test D.2. . . . .	108
6.13	Selected estimation errors of the EKF and the KF in Test D.2. . . . .	109
6.14	Selected estimation errors of the EKF linearized at the presumed configuration $\mathbf{x}_0$ and the changed configuration $\mathbf{x}_0^*$ . . . . .	109
7.1	Rotor speeds and tilting angles at hovering states specified by an axis $\mathbf{k} = (0.65 \ 0.65 \ -0.38)^\top$ and angle $\vartheta_e$ varying from 0 to $2\pi$ . . . . .	117
7.2	Intersection-search using Newton's method . . . . .	118
7.3	Flowchart of the process for saturation prediction and avoidance. . . . .	123
7.4	Scatter plot of the randomly selected target poses of Monte Carlo tests. . . . .	124
7.5	Rotor speed time series from a set of Monte Carlo tests specified by 200 random target poses. . . . .	125
7.6	Rotor acceleration time series from a set of Monte Carlo tests specified by 200 random target poses. . . . .	126
8.1	The impedance control strategy. . . . .	140
8.2	Block scheme of the axis-selective impedance and position control. . . . .	142
8.3	System response to $f_{e,z} = 5\text{ N}$ with $m_A = 5.8$ , $k_A = 80$ and varying $d_A$ . . . . .	144
8.4	System responses to $f_{e,z} = 5\text{ N}$ with $m_A = 5.8$ , $d_A = 30$ and varying $k_A$ . . . . .	144

8.5	System responses to $f_{e,z} = 5\text{ N}$ with $d_A = 30$ , $k_A = 40$ and varying $m_A$ . . . . .	145
8.6	Block diagram of the pose control with exact linearization and inverse differential kinematics. . . . .	145
8.7	Time history of the reference trajectory and the actual end-effector pose. . . . .	147
8.8	Time history of the tracking errors and the Euclidean norm. . . . .	147
8.9	Time history of the end-effector velocity and the reference in the operational space. . . . .	148
8.10	Time history of the control input. Left: control input of the UAV. Right: control input of the manipulator. . . . .	148
8.11	Time history of $\ \mathbf{P}_{G,xy}\ $ with different $k_{gp}$ and $k_{gd}$ . . . . .	149
8.12	100 steady pose references randomly generated for the end-effector. . . . .	150
8.13	Alignment error from 100 Monte Carlo runs with random initial pose. . . . .	151
8.14	Time history of the 4th joint angle with different $k_{gp}$ and $k_{gd}$ . . . . .	152
8.15	Norm of the joint errors from 100 Monte Carlo runs with random initial pose. . . . .	152
8.16	Time history of the obstacle distance with different $k_{gp}$ and $k_{gd}$ . . . . .	153
8.17	Schematic representation of the gain test for collision avoidance. . . . .	154
8.18	Sketch of Monte Carlo test for collision avoidance with $\sqrt{t_{\text{safe}}} = 0.5\text{ m}$ . . . . .	155
8.19	Results of the secondary tasks from the test with random obstacle tracks. . . . .	156
9.1	The proposed fault-tolerant control scheme in simulation. . . . .	158
9.2	Exemplary pose reference illustrated in the Cartesian space. . . . .	158
9.3	Random axes of rotation for Monte Carlo test. . . . .	161
9.4	Tracks of the tilt-hexarotor recorded from 200 random tests. . . . .	161
9.5	Selected tracking results of the FTC from a Monte Carlo run. . . . .	162
9.6	Control scheme for the integration test. . . . .	163
9.7	Time history of the position reference and the actual end-effector position. . . . .	164
9.8	Time history of the position error. . . . .	165
9.9	Time history of the COG alignment error. . . . .	165
9.10	Time history of the joint error. . . . .	166

9.11 Time history of the obstacle distance. . . . .	166
9.12 Paths of the vehicle and the end-effector visualized in $\{I\}$ . . .	167
9.13 Response of the end-effector pose to the force and torque step. . . . .	168
B.1 Proposed 6-DOF manipulator. . . . .	182
C.1 Structure of the FDI based on multiple EKFs. . . . .	185
D.1 Estimation errors of the EKF and the KF in Test A.1. . . . .	189
D.2 Estimation errors of the EKF and the KF in Test B.1. . . . .	190
D.3 Estimation errors of the EKF and the KF in Test C.1. . . . .	190
D.4 Reference and estimated wrench of the EKF and the KF in Test D.1. . . . .	191
D.5 Estimation errors of the EKF and the KF in Test D.1. . . . .	192
D.6 Reference and estimated wrench of the EKF and the KF in Test D.2. . . . .	193
D.7 Estimation errors of the EKF and the KF in Test D.2. . . . .	194
D.8 Estimation errors of the EKF linearized at $\mathbf{x}_0$ and $\mathbf{x}_0^*$ . . . . .	194



## Tabellenverzeichnis

3.1	Rotation range of the joints defined with respect to the coordinate axis specified in Fig. 3.7. . . . .	45
4.1	Experiment results of completeness and time consumption for control allocation with CMPI and IPM. . . . .	67
4.2	Experiment results of fault-tolerance for control allocation with CMPI and IPM. . . . .	69
5.1	Noise and delay of the measurement. . . . .	80
5.2	Average time consumption and FDI accuracy in single-fault test. . . . .	83
6.1	Configuration of the computer used for timing tests. . . . .	100
6.2	Noise and delay of the state estimation. . . . .	102
6.3	Configurations of the test cases. . . . .	103
6.4	Root mean square errors of the wrench observers in the case study. . . . .	111
8.1	Measurement ranges and uncertainties of the F/T-sensor . .	143
B.1	Hexarotor nominal parameters. . . . .	181
B.2	DH parameters of the serial arm. . . . .	182
B.3	DH parameters of the tool links. . . . .	182
B.4	The COM position of the links expressed in the link frame. .	183
B.5	Mass of the links. . . . .	184
B.6	Inertia matrix of the links relative to the center of mass. . .	184



## Abkürzungs- und Symbolverzeichnis

### Abbreviations

ANES	Average normalized estimation error squared
ANN	Artificial neural network
CFRP	Carbon fiber reinforced polymer
CMPI	Cascading Moore-Penrose inverse
CNN	Convolutional neural network
COG	Center of gravity
COM	Center of mass
DH	Denavit and Hartenberg convention
DLS	Damped least-square
DOF	Degree of freedom
EKF	Extended Kalman filter
ESC	Electronic speed control
FDD	Fault detection and diagnosis
FFT	Fast Fourier transform
FTC	Fault-tolerant control
IMU	Inertial measurement unit
IPM	Interior-point method
KF	Kalman filter
LMA	Levenberg-Marquardt algorithm
LP	Linear program
LQR	Linear quadratic regulator
LSM	Least square method
LSTM	Long short-term memory neural network
MFCQ	Mangasarian-Fromowitz constraint qualification
MIMO	Multi-input, multi-output
MPC	Model predictive control
MPI	Moore-Penrose inverse
NEES	Normalized estimation error squared
NIS	Normalized innovation error squared
ODE	Ordinary differential equation
QP	Quadratic programming
RMSE	Root mean square error

RNN	Recurrent neural network
SVM	Support vector machine
TCP	Tool center point
UAV	Unmanned aerial vehicle
UKF	Unscented Kalman filter
VTOL	Vertical take-off and landing
WPD	Wavelet packet decomposition

## Symbols

$\bar{u}$	Virtual input in the operational space
$\lambda$	Lagrange multiplier
$\tau_m$	Input force of the manipulator
$\theta$	Joint angle vector
$\xi$	Vector of the generalized coordinates
$C$	Centrifugal and Coriolis matrix
$D_A$	Apparent damping
$G$	Gravitational matrix
$h$	Health level vector of the rotors
$I_B$	Inertia of the entire UAV w.r.t. the COM
$J$	Jacobian matrix
$J^D$	Damped least-square of $J$
$J^W$	Weighted MPI of $J$
$K_A$	Apparent stiffness
$K_k$	Kalman gain
$M$	Generalized inertia tensor
$M_{\text{eff}}$	Control effectiveness matrix
$M_{\text{ext}}$	Static control allocation matrix
$M_A$	Apparent inertia matrix
$N_J$	Projector in the null space of $J$
$n_s$	Vector containing the square values of all rotor speeds
$O_{\text{EKF}}$	Observability matrix
$S$	Selection matrix of the hybrid pose and impedance control
$T$	Conjugate Euler angle rates matrix
$t_l$	Task vector for the preferred joint configuration
$u$	Control input of the UAV
$u_\xi$	Virtual input in the joint space
$v_T$	Twist vector of the end-effector
$W$	Weight matrix



$\mathbf{w}$	Generalized input force
$\mathbf{w}_e$	Generalized external force
$\mathbf{x}$	State vector
$\mathbf{y}$	Measurement vector
$\epsilon_k$	normalized innovation error squared
$\eta_\tau$	Torque efficiency index
$\eta_f$	Force efficiency index
$\lambda_s$	Scaling vector in emergency routine
$\mathcal{K}$	Total kinetic energy
$\mathcal{L}$	Lagrangian
$\mathcal{U}$	Total potential energy
$\psi$	Yaw angle
$\varphi$	Roll angle
$\vartheta$	Pitch angle
$b$	Torque coefficient
$e_{\text{mean}}$	Absolute mean value of errors
$g$	Gravitational acceleration
$g_m$	Manipulability measure
$k$	Thrust coefficient
$l_{LSTM}$	Sequence length of the LSTM network
$n_i$	Speed of the $i$ -th propeller
$n_+$	Extreme value of the rotor speed curve
$t_g$	Objective function for the alignment task
$t_o$	Objective function for collision avoidance
${}^A_B\mathbf{T}$	Homogeneous transformation matrix from {B} to {A}
${}^B\boldsymbol{\tau}$	Input torque expressed in {B}
${}^B\boldsymbol{\tau}_{D,i}$	Torque generated by the $i$ -th rotor expressed in {B}
${}^B\mathbf{e}_{R_i}$	Direction of the $i$ -th rotor in {B}
${}^B\mathbf{f}$	Input force expressed in {B}
${}^B\mathbf{f}_{T,i}$	Thrust generated by the $i$ -th rotor expressed in {B}
${}^B\mathbf{p}_G$	Distance between the COG of the arm and the vertical line defined by the gravity vector of the vehicle
${}^B\mathbf{p}_i$	Position of the $i$ -th link expressed in {B}
${}^B\mathbf{p}_{m,i}$	COM position of the $i$ -th link expressed in {B}
${}^I\mathbf{f}_G$	Gravity expressed in {I}
${}^I\mathbf{f}_{\text{ext}}$	External force expressed in {I}
${}^B\boldsymbol{\tau}_{\text{ext}}$	External torque expressed in {I}
${}^B\mathbf{p}_{m,B}$	Position of the COM of the UAV expressed in {B}
${}^B\mathbf{r}_i$	Position of the $i$ -th propeller expressed in {B}

*Abkürzungs- und Symbolverzeichnis*

---

${}^L_B\phi$	Euler angles represent the rotation from {B} to {A}
${}^I\mathbf{p}_B$	Origin position of {B} expressed in {I}
$\alpha_i$	Tilting angle of the $i$ -th rotor
$\boldsymbol{\omega}$	Angular velocity
${}^A_B\mathbf{R}$	Rotation matrix from {B} to {A}
$SE(n)$	Special Euclidean group with dimension $n$
$SO(n)$	Special orthogonal group with dimension $n$
$\mathbf{d}$	Vector containing all vertical and lateral components of the extended thrust formulation

# Kapitel 1

## Introduction

### 1.1 Motivation

The study on unmanned aerial vehicles (UAVs) has been a popular research topic in the past decade, and many profound developments have been established [176]. Due to the capability of reaching high-altitude workspace swiftly and covering large outdoor areas efficiently, UAVs have recently been deployed in various scenarios that hazard human beings or are too costly. By gaining from the hardware miniaturization, the increase in computational power, the advancements in computer vision and control techniques, UAVs have been made possible as consumer products, and their usability and potential are manifested in an enormous public interest. The market of UAVs for commercial use was even valued as high as \$ 13.44 billion in 2020 [62]. The most common application for UAVs, both in military and civilian, is to gather vision or other stereo information from the vehicle in the observational field.

Nevertheless, the potential of UAVs can be further developed by migrating from passive tasks like reconnaissance and remote sensing to active tasks involving physical interaction between the robot and objects in its environment, i.e., aerial manipulation. This promises to present new opportunities and open a wide range of possible applications where aerial robots could be deployed for construction and maintenance on inaccessible and complex structures, thus reducing costs and risks to humans. For example, cleaning large-scale solar panels, repairing wind turbine blades, maintaining high-voltage power lines, and pipeline inspections (see Fig. 1.1) are foreseeable industry and service applications of aerial manipulation.

Physical interaction such as grasping or manipulation constitutes a particularly challenging scenario for aerial robots due to the intrinsic instability and typical underactuation. Aerial manipulation requires a vertical take-off and landing (VTOL) floating base to perform agile maneuvers and to exert precise forces on the environment in any direction while at the same time rejecting other sources of disturbance. The construction of most concurrent



(a) Photovoltaic power station in the Kubuqi Desert.



(b) Maintenance personnel are repairing a wind turbine blade.



(c) Zhangbei-Xiongan 1000kV UHV Transmission Line.



(d) Pipes of a petrochemical plant.

**Abbildung 1.1:** Examples of potential application scenarios for aerial manipulation.

VTOL UAVs is based on a co-planar multirotor design, where the rotor axes are parallel to the vertical axis of the vehicle. This design has been proved through many years and enjoys the benefits of simple and robust construction and optimal thrust efficiency when hovering. The innate coupling of orientation and position is the drawback that makes the conventional design unsuitable for aerial manipulation. On the other hand, fully actuated multirotors can compensate for torques and forces caused by the contact and orient themselves and onboard tools to perform manipulation tasks on the surfaces of complex structures, as exemplified in Fig. 1.1. Additionally, complex use cases require a high fidelity and fault tolerance under the preservation of omnidirectional maneuverability. In the event of an unexpected loss of thrust, e.g., due to propeller damage, it is desired that the vehicle can still be safely operated and landed. Consequently, aerial vehicles should be configured with redundancy to tolerate partial, single, or even multiple effector failures.

To endow aerial vehicles with sufficient manipulability for “tactile” tasks,

combining a fully actuated multirotor UAV with a multi-joint manipulator becomes relevant. The resulting system inherits unlimited mobility from the UAV and dexterity from the robotic manipulator. Therefore, aerial manipulation can be considered the natural evolution of mobile robotics, adding manipulation capabilities to the agility and versatility of VTOL UAVs. There is no doubt that aerial manipulators will improve the quality of work distributed over a wide area or in hazardous conditions and situations. Nevertheless, the question remains how to develop accurate and reliable interaction control in six degrees of freedom (DOF) for a complex floating multi-body system.

## 1.2 Research Objectives

This dissertation aims at developing an aerial platform and control solutions motivated explicitly by aerial manipulation. In particular, this work will design an aerial manipulator consisting of tiltable rotors and serial rotational joints and focus on developing hybrid pose and impedance control for the platform subject to constraints in realistic conditions. By considering individual elements which constitute the whole control loop, objectives are listed as:

- Design of the aerial manipulator as a combination of a tailor-made manipulator for a floating base and a multirotor UAV extended with the capabilities of full actuation.
- Controllability and observability analysis for the proposed aerial manipulator.
- Risk minimization of input saturation in an early stage since it is the most undesired situation which endangers the system stability.
- Active fault-tolerant control is to be developed for a single fault during free flight, where the system model can be simplified. As a prerequisite, thrust loss has to be detected and isolated correctly. It could also be helpful to estimate the severity of the fault.
- Compliant behavior of the end-effector along a specific direction is necessary for soft contact during a manipulation task. Based on the knowledge of external forces and torques provided by an observer or a force/torque sensor, this objective can be achieved by axis-selective hybrid pose and impedance control.

- Apart from the primary control objective, redundancy of the proposed aerial manipulator can be exploited to accomplish a set of secondary tasks, which are ordered according to their priority.
- Despite the focus on a particular aerial manipulator, the work should be presented in an application-agnostic manner whenever possible to ease the transfer to other redundant aerial manipulation systems with flat dynamics.

## 1.3 State of the Art

### 1.3.1 Aerial Manipulation

Aerial robots have been either equipped with a gripper or a multi-fingered hand rigidly attached to the aerial robot fuselage (e.g., [5, 58, 99, 128]) or complex manipulators (see [89, 143, 167, 172]) to accomplish manipulation tasks in the air. Fig. 1.2 shows examples for both solutions. Lightweight



(a) Yale Aerial Manipulator equipped with a gripper [12].



(b) Helicopter equipped with a 7-DOF manipulator [89].

**Abbildung 1.2:** Examples of two solutions for aerial manipulation.

low-complexity grippers are implemented following the first solution for multirotors [99, 107] and helicopters [12]. A low-cost solution is discussed in [60]. Fixed tools in the first approach do not bring extra DOF to the whole system. Due to lack of dexterity, this approach is commonly used for simple tasks such as pick and place [184], pushing [128], and door opening [175].

Linking the object to an aerial vehicle through tether mechanisms can be classified as another possible solution. Cable-suspended load-lifting by a quadrotor is addressed in [40]. Foehn u. a. [50] present a fast trajectory optimization algorithm for quadrotors with a cable-suspended payload. Transporting the payload by multiple aerial robots via cables is discussed in [16, 109, 164].

In contrast, aerial robots equipped with manipulators can accomplish more complicated aerial manipulation tasks. The robotic arm of an aerial manipulator plays a crucial role in its functionality. The manipulator can be categorized based on the configuration. The choice of the parallel structure is motivated by its high stiffness. A 6-DOF parallel manipulator, which allows for little moving mass, and is easily stowed below a quadrotor, is presented in [41], while Kamel, Alexis und Siegwart [82] introduce a 3-DOF parallel manipulator. Lightweight Delta manipulators, capable of pure translational motion, are used in [38, 79]. Serial manipulators, characterized by their open kinematic chains, have a relatively higher workspace/robot-size ratio. In [167], an anthropomorphic dual-arm is designed for aerial manipulation. Fig. 1.3 shows three examples of manipulator configuration. The existing

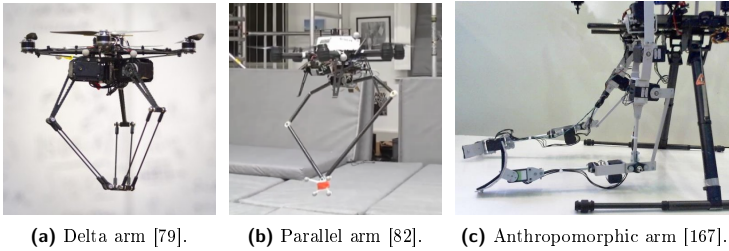


**Abbildung 1.3:** Examples of manipulator configuration.

designs can be distinguished alternatively by the number of the arm-DOF: 1-DOF [192], 2-DOF [57, 85, 172], 3-DOF [86, 87, 90, 118], 5-DOF [15], 6-DOF [30] or more [65, 89]. It is preferable to minimize the overall system inertia by raising the COM of the manipulator closer to the UAV's COM. Wuthier u. a. [186] proposed a compact aerial manipulator design, which assigns all motors in the base. Mechanical power is transmitted from the motors to the joints via timing belt and pulleys mechanism (see Fig. 1.4a). Honeycomb structure (see Fig. 1.4b) is used in [15] to reduce the total weight. The compliance can reduce the effect of the physical interaction with the environment on UAV stability, and it is achieved in [166] by integrating a transmission mechanism consisting of a pair of compression springs between the servo shaft and the output frame (see Fig. 1.4d).

Overall, employing the tools, the object can be grasped and locally manipulated during the flight. Unfortunately, the single gripper is not enough

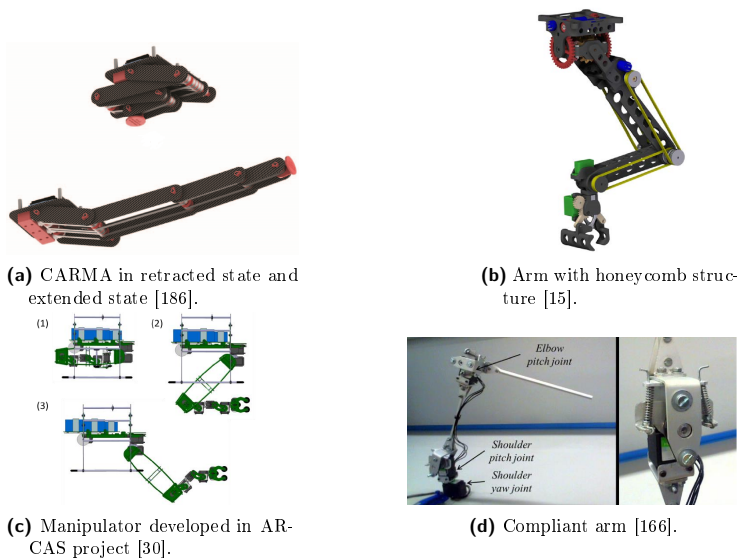


**Abbildung 1.4:** Examples of manipulator design.

to obtain a complete evolution from passive to active manipulation tasks. The approach involving complex manipulators could be a better solution for active tasks since it provides an aerial vehicle capable of performing dexterous actions. In the past few years, we have seen the development of UAVs equipped with simple grippers towards highly complex  $n$ -DOF manipulators. AEROARMS<sup>1</sup> is a European project focusing on aerial robots for outdoor industrial inspection and maintenance; Developed aerial robotic manipulation technologies and methods are summarized in [123]. Several aerial manipulators were also presented and demonstrated for applications such as drawer opening [87], valve turning [92], and pipe inspection [103]. A brief literature review of aerial manipulation up to 2018 was carried out by Ruggiero, Lippiello und Ollero [145].

---

<sup>1</sup><https://aeroarms-project.eu/>



### 1.3.2 Fully Actuated UAVs

The generic multirotor UAVs with collinear rotors show their limitation in the scenarios where the UAV has to interact physically with the environment. In particular, the underactuated multirotor cannot exert any force parallel to the plane perpendicular to the body's vertical axis, so that its attitude has to be changed for lateral motion. Therefore, underactuation limits the possible physical interactions to exchange forces along the three axes and torques around the vertical axis. It has been shown that in the presence of interactions with points of the structure other than the COM, the internal dynamics of underactuated multirotors are not guaranteed to be stable and are not, in general, easy to stabilize [119].

Diverse concepts for fully actuated aerial vehicles have been proposed to tackle this fundamental limitation that can hover at arbitrary orientations and change its position regardless of its current orientation. The ability to exert a full-DOF force and torque decouples the translational and rotational dynamics, enabling precise interaction with the environment while maintaining stability. Generally, full-actuation is achieved by a proper design of the propeller positions and orientations. In [153], the issue is addressed by four additional rotors at the end of each frame in lateral position. Nevertheless, the position of the rotor increased the complexity of controllability because of the airflow between the vertical and the lateral rotors, resulting in nonlinear dynamics. In general, it is possible to classify fully actuated UAVs based on their propeller configuration.

**UAVs with Fixedly Tilted Rotors** One way to implement a fully actuated multirotor is to mount tilted rotors [148] as shown in Fig. 1.5a such that the thrust of each propeller is not collinear anymore. If the number of propellers is at least six and tilting directions do not generate a singular configuration, it is then possible to control the force vector at will (inside the input envelope) by selecting the intensity of the thrust produced by each propeller. This method has the benefit that little additional hardware is needed compared to a conventional collinear hexarotor, and these vehicles tend to inherit the advantage of low complexity that has made conventional multirotors successful. The optimization of tilting angles has been introduced in [88, 139, 140, 168], which considered different optimization parameters. Schuster u. a. [154] compared design approaches based on maximum wrench generation and minimum energy consumption. Rashad u. a. [140] emphasized the need for bi-directional propellers on vehicles with fixed rotor angles to achieve a

truly omnidirectional UAV. The ability to reverse the thrust of the motors can be achieved with variable-pitch propellers [84, 94] or by having ESCs with direction control [130].

**UAVs with Tilting Mechanisms** In this case, the configuration is changing during operation due to additional tilting mechanisms. The quadrotor design with four additional servo motors included for the tilting [48, 146] provides versatility in force generation and efficiency but without pose-omnidirectionality. The control scheme proposed in [146] allows the quadrotor to hover at a maximum pitch angle of  $25^\circ$ . Even though the vehicle showed the ability for a 6-DOF flight, the limited speed of the servo motors and the additional weight caused the system to be hard to control. Another hexarotor with the ability to tilt all rotors synchronously was presented by Ryll, Bicego und Franchi [147] in Fig. 1.5b. This vehicle aims to take the best of two worlds by combining the efficient flight of an underactuated UAV with the supreme accuracy and tracking abilities of a fully actuated aerial vehicle. In [81], the rotors are tilted by BLDC motors mounted within the arms of the vehicle (see Fig. 1.5c) and represent a significant improvement in speed and range of motion compared to previous designs using servomotors [146]. The tilting mechanism also enables the aerial vehicle to adjust the directi-



(a) Tilt-Hex [148].



(b) FAST-Hex [147].



(c) Voliro [81].

**Abbildung 1.5:** Examples of Fully actuated UAVs with tilted rotors.

on of individual thrust to improve efficiency drastically when hovering at a non-zero pitch/roll orientation. However, these benefits come at the cost of higher complexity and weight.

**UAVs with Unconventional Geometries** In addition to UAVs building on a conventional design, some more exotic vehicles have been presented. These vehicles feature an unconventional geometry and aim to improve certain aspects of the performance of a fully actuated aerial robot. Primarily,

these designs emphasize maneuverability and can have benefits over more traditional designs in particular applications. Using an optimized geometric configuration of 8 fixed rotors, a cube-shaped omnidirectional UAV [28] can produce the same magnitude of forces and moments equally in all directions. This concept maximizes the flight envelope but sacrifices energy efficiency, as only some rotors are working parallel to the gravity vector in any given orientation. Another concept is the ODAR UAV presented by Park u. a. [130], consisting of eight bi-directional propellers mounted to a single central bar. The authors have reported a full flight envelope and mentioned the possibility of exerting downward pushing force larger than its weight.

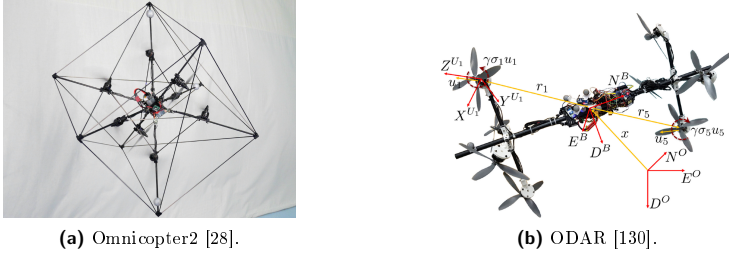


**Abbildung 1.6:** Examples of fully actuated UAVs with unconventional geometric structures.

The vehicle's flight envelope is the range of aerodynamic parameters such as speed, attitude, altitude, and load factor<sup>2</sup> in which the vehicle is aerodynamically stable. For fully actuated UAVs, the term assesses vehicle's maneuverability and primarily describes the range of orientations the vehicle can maintain a hovering position. The reachable force envelope is visualized for the designs mentioned above in [7, 52].

### 1.3.3 Control Strategies of Multirotors

During manipulating operations, the motion of the arm involves changes in the position of the center of gravity (COG). The physical interaction with the environment also generates forces and torques, which depend on the actual configuration of the aerial manipulator. Together with the intrinsically

<sup>2</sup>In aeronautics the load factor is the ratio of the vehicle's lift to its weight.

unstable dynamics of the aerial vehicles, such challenges have to be addressed by the controller to complete aerial manipulation tasks successfully.

Diverse control approaches designed for aerial manipulation systems can be classified into two categories. The first category consists of decentralized approaches. The aerial vehicle and the manipulator are considered two separate subsystems with their own control loops. Coupling effects are handled either by feedback as external disturbances or by feedforward based on decoupling techniques. In the other category, centralized controllers are designed based on the complete kinematic and dynamic models of the aerial manipulator. In this case, the aerial platform and the arm are considered a unique entity: a multi-body system.

### **Decentralized Control**

If the UAV and the attached manipulator are seen as two separate systems, the modeling and control problems are addressed individually. Methods for modeling, planning, and controlling the sole manipulator are well established and detailed illustrated in many textbooks [157, 158, 162]. One can use the mature manipulator control techniques as the inspiration for aerial manipulator control while keeping in mind the fundamental difference of the floating base.

Regarding the aerial platform, the control problem of underactuated quadrotors has been well researched with linear control approaches (e.g., [26, 112, 115, 170, 183]). Nonlinear control approaches, including backstepping [27, 104, 193],  $\mathcal{H}_\infty$  method [137], sliding mode control [17, 187], nested saturation [31], model predictive control (MPC) [6], have been applied as well. Fumagalli und Carloni [55] have proposed a modified impedance control strategy for the physical interaction of UAVs and validated it in experiments on a real quadrotor flying vehicle. The dependence of thrust on the angle of attack, airflow disruptions, and blade flapping has been studied in [68, 72]. It has been shown that these effects significantly influence fast maneuvering and should be mentioned in controller development for aggressive flight maneuvers [71]. Geometric PID control on  $SE(3)$  ([84, 140]), exact linearization ([39, 139]), and integral sliding mode control [189] are known approaches applied to fully actuated hexarotors with nonparallel tilted rotors. An adaptive backstepping controller is used to control a UAV with an unconventional structure in [121].

Utilizing the redundant DOF of the Kuka LWR, the partial decoupling between helicopter and arm is achieved in [73] by means of restricting the

movement of arm COG in the lateral plane of the helicopter. Ruggiero u. a. [144] have employed an estimator to compensate unmodeled dynamics and external wrench acting on the aerial vehicle. A moving battery is used in [143] to counterweight the statics of the robotic arm.

### Centralized Control

As the basis for centralized control approaches, the kinematic and dynamic models of the whole aerial manipulator need to be derived first. When it comes to dynamic modeling, two approaches are applied commonly: the Euler-Lagrangian formalism and Newton-Euler recursive formulation. In [100], the dynamic model of a UAV with an attached robotic arm is derived in a symbolic matrix form through the Euler-Lagrangian formalism. Kannan, Olivares-Mendez und Voos [83] have modeled an aerial manipulator with the Newton-Euler approach. The adaptive control approach in [9] is based on the recursive Newton-Euler formulation.

Several control schemes have been developed to address the control problems for aerial manipulation. Kim, Choi und Kim [85] have demonstrated an adaptive sliding mode controller in an experiment including picking up and delivering an object using a quadrotor with a 2-DOF arm. Yang u. a. [188] have designed a full-state feedback linear quadratic regulator (LQR) controller and revealed an underlying structure of the centralized dynamics that helps the control design. Output feedback linearization and stable zero dynamics are exploited in [108]. Orsag, Korpela und Oh [126] und Orsag u. a. [127] have presented a control scheme to achieve dynamic stability in a mobile manipulating unmanned aerial vehicle using a combination of gain scheduling and Lyapunov based model reference adaptive control. Another hierarchical motion control scheme is proposed in [10] for a quadrotor UAV equipped with a manipulator. A multi-level impedance control scheme for aerial robotic manipulators is proposed in [32]. The outer loop is composed of a trajectory generator and an impedance filter that modifies the trajectory based on the force/torque feedback provided by a sensor mounted on the wrist to achieve a compliant behavior; a middle loop is used to solve inverse kinematics; finally, the inner loop is aimed at ensuring the motion tracking. Depending on the employed UAV and manipulator, the mechanical system may be redundant for the given task. Therefore, a Cartesian impedance control with redundancy resolution is described in [100]. However, even if the whole aerial manipulator is redundant for the task, the underactuation problem regarding the underactuated UAV persists.

Following centralized approaches, aerial manipulators are employed in several applications. Korpela, Orsag und Oh [91] have developed a test rig incorporating the dynamic and kinematic model for a mobile manipulating UAV. The end-effector pose combines the six DOFs of the emulated aircraft, seven DOFs of the manipulator, and four DOFs for the hand. A series of hole insertion experiments were performed for model verification. In [90], a dual-arm manipulator is used for an aerial valve turning task. A sequential Newton method for unconstrained optimal control is used in [57] for model-predictive control in aerial pick-and-place tasks. Experiments including opening and closing an unknown drawer using an aerial manipulator have also been conducted [87].

### 1.3.4 Control Allocation

As one of the effective accommodation techniques for controlling over-actuated systems [45], the control allocation approach offers the advantage of modular design. The design of the high-level control strategy is independent of the actuator configuration by introducing the virtual control module and control allocation module, respectively. As shown in Fig. 1.7, the motion control algorithm of over-actuated mechanical systems is organized hierarchically in three layers. A high-level controller represents the top layer which compu-

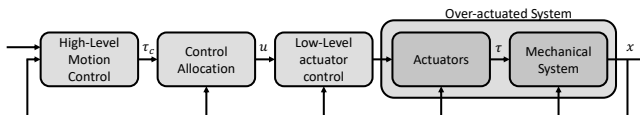


**Abbildung 1.7:** Control system structure using control allocation.

tes the desired control wrench (force and torque) in body-fixed coordinates of the mechanical system to meet the overall control objectives. The commanded virtual input vector is mapped to individual actuators by a control allocation algorithm. The computed motor commands are eventually fed into the motor controllers, which form the lowest level of the control algorithm hierarchy.

The primary task of the control allocation is defined as minimizing the allocation errors under the given effectiveness of the propulsion system without saturating any actuator. The allocation algorithm can also handle secondary objectives such as power efficiency and tear-and-wear minimization. This

is frequently solved by deriving a (quasi-)static control allocation problem and computing the exact solution at each iteration of the control loop (e.g., [23, 24, 169]). If the system is inherently nonlinear, it is either linearized by evaluating its Jacobian matrix or linearized by means of a nonlinear input transformation that eliminates the system's nonlinearities. Johansen und Fossen [78] provided a survey of control allocation algorithms classified based on the use of linear or nonlinear models.

The easiest solution to the static mapping problem is applying a Moore-Penrose Inverse (MPI), e.g., [61, 69]. Due to the non-square effectiveness matrix of over-actuated systems, the generalized inverse is used to solve this problem using the least square method (LSM). This allows computing analytical solutions using numerical linear algebra [46, 51, 125, 159]. However, the minimization of the sum of squared inputs does not guarantee that constraints on individual actuators are satisfied. Shi u. a. [156] tackle this issue with redistributed pseudo-inverse, which projects the unconstrained optimal control vector onto the admissible set. The unsaturated elements of the input vector are re-computed by solving a reduced problem using a reduced pseudo-inverse. The daisy-chaining method [3, 124] offers a less effective but straightforward alternative by grouping the effectors into ranked groups. The control allocation problem is solved in order of priority, and it may lead to solutions where several effectors are not fully utilized to minimize the allocation error and be suboptimal compared to the redistributed pseudo-inverse.

Due to the request to handle more challenging formulations with nonlinear models or complex constraints and objectives, there has recently been increasing interest in iterative numerical optimization procedures since their computational complexity is already within the capabilities of today's off-the-shelf embedded computer technology. With the cost function defined by either 1-norm or  $\infty$ -norm, the control allocation is reformulated into a linear program (LP) in [20, 21, 129]. A cost function with  $\infty$ -norm minimizes the maximum effector use and therefore balances the wear of actuators [21]. Using 2-norm as the cost, Johansen, Fossen und Berge [76] have formed the control allocation problem as a quadratic program (QP). Wang, Yi und Fan [180] extended a QP by adding an additional term to penalize the actuator rates, where the control allocation result also depends on the previous distribution. In the context of control allocation, the most common numerical methods for LP and QP are the *simplex method* [20], *active set method* [63], and *interior-point method* [133].

The main problem in static control allocation is its computational burden due to the numerical solution of the constrained optimization problem at

each sampling instant. It is hard to guarantee the limit of the number of iterations. The control allocation may have to accept a certain degree of suboptimality since the maximum number of iterations is limited in real-time implementation. Dynamic control allocation methods are developed to deal with this difficulty, where a dynamic update law is derived instead of solving an optimization problem at each instant. This reduces the computational intensity compared to optimization algorithms that might not find a feasible solution within the given time. Introducing a dynamic Lyapunov-Control law, Johansen [77] proposed an algorithm for slow-moving maritime vessels, which asymptotically tracks the optimal allocation. Dynamic inversion technique is used in [98], which is based on a Lyapunov design approach with finite-time convergence to optimality. Using Lyapunov analysis for cascaded set-stable systems, uniform global/local asymptotic stability is guaranteed for the sets described by the system, the optimal allocation update-law, and the adaptive update-law in [171]. In [56], a systematic method for closed-loop dynamic control allocation is proposed, and aircraft stability analysis is introduced. The dynamic control allocation is only asymptotically optimal. As shown in the case study in [169], this leads to performance degradation.

### 1.3.5 UAV Fault-Tolerant Control

Fault-tolerant capability is a beneficial feature for multicopter systems to improve reliability and safety. Fault-tolerant control (FTC) aims at preventing a component fault<sup>3</sup> from causing a failure<sup>4</sup> at the system level [19]. The FTC can control the system with satisfactory performance even if one or several faults, or more critically, one or several failures occur in this system [45]. The active FTC scheme consists of two parts: a) the diagnosis unit detects, isolates, and estimates the fault; b) the reconfiguration unit adapts the controller according to the faulty situation to maintain the overall system performance.

**Fault detection:** The system is able to detect the fault when a fault occurs.

**Fault isolation:** The system is able to tell where or on which part the fault occurs.

---

<sup>3</sup>In the context of FTC, a fault is an unpermitted deviation of at least one characteristic property (feature) of the system from the acceptable, usual, standard condition [74].

<sup>4</sup>In the context of FTC, a failure is a permanent interruption of a system's ability to perform a required function under specified operating conditions [74].



**Fault estimation/identification:** The system is able to estimate the severity of the fault.

**Control reconfiguration:** The controller is reconfigured so that the overall system continues to satisfy its goal.

An overview of the existing works on fault detection and diagnosis (FDD) and fault-tolerant control is presented in [194] for quadrotor systems. However, due to the configuration of a quadrotor vehicle, it lacks actuator redundancy that is necessary for fault tolerance without downgrading the control performance. Any rotor failure will cause the quadrotor to become uncontrollable. Therefore, most studies on quadrotor systems are either limited to FDD [35, 36, 195] or only consider the partial loss of control effectiveness fault in actuators [97, 155]. The total failure was studied in [53, 117], where the yaw motion control is sacrificed. In [18], the fault is only detected based on the Kalman filter (KF) but not isolated and estimated. Wang und Puig [182] have used zonotopic extended Kalman filter (EKF) for fault detection. However, fault isolation is not considered in their research.

Hexacopters and Octocopters are more suitable for FTC design due to the available physical redundancy for the 4-DOF motion control. System reliability and safety are improved significantly due to redundant rotors. The reconfigurability of multirotor vehicles is analyzed in [44, 178]. A fault detection and reconstruction scheme is established in [181] for hexarotor vehicles. For every actuator, an EKF-based observer is equipped to estimate the lift factor, and the fault is detected and isolated by analyzing this lift factor. Vey und Lunze [177], on the contrary, use seven EKFs for their FTC scheme. One observer is responsible for fault detection, and the other six are for fault isolation. According to the diagnosis, a control reconfiguration is constructed. Fault estimation is not taken into account in their method. The flatness technique has been used in [152] to detect sensor and actuator faults. In [150, 151], FDI approaches based on nonlinear observers are presented for an octocopter with a coaxial configuration. If a rotor encounters fault or failure, a counteraction on its dual-motor compensates for the loss of thrust. Accommodation strategies based on linear parameter varying [8], sliding mode control [179], and cascade pseudo-inverse [105] are proposed for octocopters in case of rotor failures. These papers consider only the recovery part of the FTC by assuming available fault information.

In addition to model-based approaches, data-driven methods based on artificial neural networks (ANN) are also researched for FTC. Utilizing a support vector machine (SVM) as the FDI solution, Jun und Tian [80] adapt

the parameters in the control loop of a quadrotor according to the diagnosis result. However, SVM is a traditional machine learning method, the general performance of which can be improved indeed. Another traditional machine learning method, random forest classifier, is used in [134]. They only focus on the fault that occurs on the motor rather than the propeller, which can be easily detected by measuring motor current for an aerial manipulator. Fu u. a. [54] have proposed a hybrid convolutional and long short-term memory neural network (CNN-LSTM) model for a regular Hexarotor. One significant flaw of their method is a diagnostic delay over 200 ms. Yousefi u. a. [191] use linear discriminant analysis and logistic regression as machine learning algorithms in their research. Nevertheless, they did not consider the isolation process. Jiang u. a. [75] claim that they are the first to involve signal processing techniques in the FDI of the actuators of the UAV. Before feeding input data into a machine learning algorithm, they use wavelet packet decomposition (WPD) to preprocess the sensor signal. Bondyra u. a. [22] use the WPD and fast Fourier transform (FFT) for preprocessing. The signal is then forwarded to an SVM. Cheng u. a. [37] introduce an active fault-tolerant controller for UAV's attitude using a non-singular fast terminal sliding mode control technique, where an ANN-based fault estimation observer is designed to obtain the actuator fault and external disturbance. They use the radial basis function to build the neural network. In this case, the mathematical description is required to implement the observer-based algorithm. Qian, Jiang und Liu [135] also designed an FTC system of a UAV for attitude control. The fault diagnostic component can detect and estimate actuator faults, and a nonlinear fault detection observer is developed to achieve this. Similar to [37], mathematical modeling is also required. One notable and exciting piece of research by Liu, Chen und Zheng [101] is based on the audio signal. This method collects audio signals by specific sensors and converts them to a spectrogram. Broken propellers generate different spectrograms. With the help of CNN, the trained model can achieve FDI. The accuracy in their experiments is higher than 90%. Unlike model-based approaches, fault estimation is relatively uncommon in data-driven approaches.

All studies mentioned previously are carried out for regular underactuated multirotors. In [110, 111], a set of algebraic conditions is provided for fully actuated multirotors with any number of generically oriented rotors to ensure static hover. To the best of the author's knowledge, no complete FTC scheme has yet been developed for a fully or over-actuated multirotor.

### 1.3.6 Input Constraint Considerations

Due to the bounded rotor speed, tilted hexarotors are subject to state and input constraints. In the case of the saturation in such a nonlinear system, the control authority is degraded, i.e., affected components of the 6D pose can not be controlled independently anymore, which further induces such a problem that the trajectory cannot be fully tracked. In worse cases, the UAV becomes uncontrollable and crashes. An approach is proposed by Lai, Wang und Chen [93] for an underactuated quadcopter. It is based on B-splines for a 3D trajectory design. It is assumed that the rotation of the system can be expressed as a function of the translational velocity. Consequently, it is not relevant to fully-actuated vehicles. Another work generates trajectory iteratively via the *Direct Adjoint Approach*, and the output parameters are adjusted until the result meets the dynamic limitations of the quadcopter [64]. To cope with the input saturation, customized flight control was researched by Nicotra, Naldi und Garone [120] and Convens u. a. [39]. A prefilter called *Explicit Reference Governor* is prefixed to the control loop and manipulates a given reference trajectory online depending on the system state to avoid input saturation. Franchi u. a. [52] present a geometric controller for tilted hexarotors. It ignores the attitude components in the case of impracticability of a reference trajectory and only follows the translational reference.

### 1.3.7 Wrench Observer

Force control is usually applied for aerial manipulation tasks, which requires knowledge about the external force and torque values acting on the tool center point (TCP) when in contact with the environment [148]. The required external wrench can be measured by a force/torque (F/T) sensor or estimated by an F/T observer. Although a sensor provides a good and reliable measurement, it increases the cost and weight of the platform and only measures the wrench applied to the point where it is mounted. A well-designed wrench observer provides an adequately precise estimation at a reduced cost, weight, and power consumption [190]. Compared to a force/torque sensor, an observer requires no additional hardware, making the whole system cheaper and more lightweight. Instead, the observer requires a mathematical model of the platform, measurements of onboard sensors as well as knowledge about the wrench generated by the rotors of the UAV [174]. Furthermore, one can estimate the wrench applied to any point of the platform.

The momentum-based observer was inspired by a nonlinear disturbance

observer used for robotic manipulators [114]. This general approach was presented for underactuated [102, 142, 190] as well as for fully-actuated [138, 144, 148] multirotors. Regarding the aerial platform and the manipulator as two separated systems instead of one entire entity, Ruggiero u. a. [143] applied the approach to an aerial manipulator with the purpose of compensating the dynamic effect of the attached manipulator on the multirotor. The drawback of the momentum-based observer is the assumption that the time derivative of the external forces is zero and, therefore, rapidly varying external forces will lead to poor estimation. It is challenging to obtain the required drift-free translational velocity of a UAV, and this would also restrict the application of the momentum-based observer. Tomić and Haddadin [173] proposed a hybrid observer to improve the UAV's behavior upon collisions, relying only on directly measured values from an inertial measurement unit (IMU). An acceleration-based method estimates the external forces, while the external torques are estimated using the momentum-based concept. Because the external wrench is assumed to be constant during one estimation step, the same problem as for the momentum-based observer occurs when quickly changing external wrenches are acting on the aerial platform. Cayero, Morcego und Cugeró [33] applied a Kalman filter to a quadrotor and pointed out the importance of the acceleration measurements due to the Kalman filter's superior performance, including the acceleration measurements. Another observer design based on an EKF was presented by Cayero Becerra, Cugeró Escofet und Morcego Seix [34] for a planar quadrotor. Baetz u. a. [13] proved that an extension of the measurement vector by acceleration measurements results in a significantly improved performance for a manipulator. Furthermore, the observers based on extended or unscented Kalman filter (UKF) show nearly the same performance. In [185], different observers from the above three groups are evaluated for an aerial manipulator with a 3-DOF manipulator attached to a hexarotor with variable tilted rotors. It has appeared that the EKF provides a more accurate estimation with concurrent good noise suppression and high dynamics. Camoriano u. a. [29] presented an incremental semiparametric approach. The nonparametric modeling is based on machine learning.

## **1.4 Scientific Contributions**

In this work, a novel solution is presented for the overall control of the aerial manipulator. The contributions are summarized in four groups in Fig.

1.8. It is worth mentioning that all the results are formulated in a general way to be applied to any specific platform configuration, as long as the necessary redundancy is available inside the aerial manipulator. For the sake of transparency of the design results, a suitable reference configuration (see the following contribution and Chapter 3) is used through the thesis, which is established as a universal platform to perform various aerial manipulation tasks.

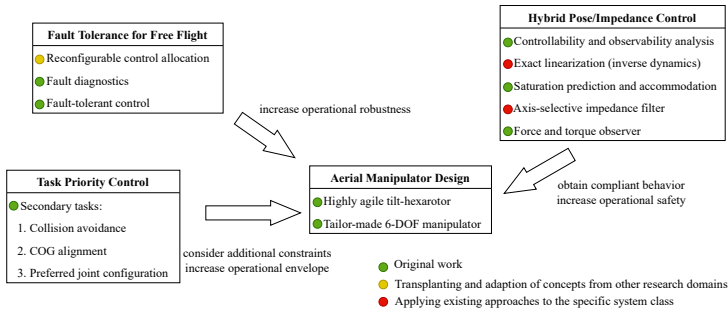


Abbildung 1.8: Overview of the contributions and benefits.

**Aerial manipulator design** In order to provide a sufficient flight envelope, this thesis adopts the tilt-hexarotor concept for the flying base. Evolving from regular underactuated hexarotor design with collinear rotors, the highly agile tilt-hexarotor possesses a mechanism for tilting the individual rotors around their axes. This concept comes with the drawback of a more complex multi-rotor system but is beneficial in several points. The ability to generate forces and torques in arbitrary directions makes the tilt-hexarotor fully actuated with an omnidirectional flight envelope. To the best of found knowledge, the proposed design is the most efficient among all the fully actuated multirotors despite reduced efficiency compared to common commercially available multirotors due to counteracting forces. Moreover, there is free space on the top and bottom of the fuselage for accessories, and the manipulator can be easily mounted. Last but not least, the tilt-hexarotor provides actuator redundancy utilized by the control allocation for energy minimization and fault tolerance. Subject to the constraints related to aerial manipulation, a dexterous, fully

stowable 6-DOF manipulator has been designed to have low weight, a simple structure, and enough strength. Manipulability is evaluated as well.

**Hybrid pose and impedance control** As a prerequisite of the control design, the controllability of the nonlinear system is verified by proving that the aerial manipulator is differentially flat. Therefore, the high-dimensional, nonlinear system can be dynamically linearized in the joint space. The operational space is linked to the joint space via the (inverse) differential kinematics equation. Consequently, the motion of the end-effector can be controlled in the operational space.

While previously published studies considering input constraints of fully-actuated UAVs tend to customize the control loop, this work introduces an alternative concept to generate saturation-free trajectories for free flight by studying the tilt-hexarotor with bounded rotor speed and acceleration. If any saturation is predicted, the trajectories are adjusted to ensure the feasibility of the reference transferred to the subsequent control loop. Compared to existing approaches, the requirements and complexity of flight controllers are reduced by the trade-off of increasing the complexity of the trajectory generator. Considering that trajectories are calculated offline, the system benefits from a lower control delay.

Compliant behavior of the system is desired to increase the operational safety of manipulation tasks. The axis-selective impedance control is employed as an outer control loop to achieve this behavior that allows the apparent inertia, damping, and stiffness to be modified as needed. This approach allows smooth switching between impedance and position control since the impedance control acts as a simple pass-through in the overall control scheme. The operational space is divided into an impedance/force-controlled subspace and a position-controlled subspace. The end-effector reveals compliant property in specified dimensions while keeping rigid in other dimensions.

Furthermore, a force and torque observer is necessary to provide knowledge of the forces and torques acting on the end-effector to the impedance controller. While the vast majority of related researches presumed only UAVs without a manipulator, the force/torque estimation for an entire aerial manipulation system consisting of both a floating base and a manipulator has been researched in this work. Two filter-based observers are presented: an EKF-based observer and a KF-based observer. Accordingly, the aerial manipulator is modeled as a nonlinear and a linear model, respectively. Although the Euler-Lagrange method is theoretically usable to derive the dynamic mo-

del, it is challenging to apply it for high-DOF aerial manipulation systems in practice due to the complex calculation of derivative matrices. In the present work, the high-dimensional computing process is decomposed mathematically, and the derivatives are derived using a numerical method to meet the real-time requirement. Both state-space models are studied for observability. To the best of the author's knowledge, this is the first time the observability analysis and consistency test have been carried out for the force/torque estimation on an aerial manipulator.

**Fault-tolerant control for free flight** Fault tolerance during the free flight is presented as the main result of this contribution. Due to the redundancy of the tilt-hexarotor, the proposed control scheme can tolerate one or more effector faults depending on the power of individual propulsion units. In specific, the active fault-tolerant control is achieved by integrating a diagnostic module, including fault detection, isolation, and estimation, into the control loop of the aerial manipulator in free-flight mode (see Fig. 1.9). The successful Monte Carlo simulations indicate that this work fills a gap in the fault-tolerant control of fully-actuated aerial platforms without sacrificing the controllability in any dimension.

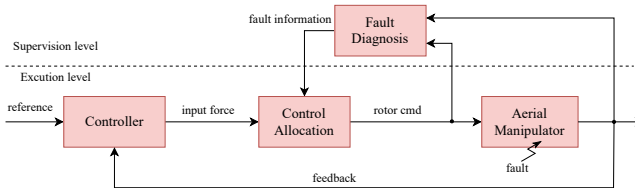


**Abbildung 1.9:** Architecture of the proposed active fault-tolerant control.

Inspired by the studies [191] and [54] done for collinear multirotors, a data-driven diagnostic approach has been developed in this thesis for the omnidirectional aerial manipulator during a free flight. In contrast to the existing filter-based methods, it does not require any precise knowledge of the mathematical model. Thanks to the redundant tilt-hexarotor design, up to two effector failures can be tolerated theoretically. Accordingly, this thesis innovatively proposes an LSTM-based solution for the FDI by expanding the prediction classes from a single fault to two faults and modifying the classification problem to a regression problem. Furthermore, a fault estimation

procedure can provide an indicator defined in the range  $[0, 1]$  to describe the severity of the fault in case of partial loss of the control effectiveness. The performance of the diagnostic module is assessed and compared with a model-based approach in a series of simulations using Monte Carlo method. The comparable accuracy and much shorter isolation time give the proposed method the dominant position in the comparison.

The faults are accommodated by a control allocation module, which takes the diagnosis as input, and recovers the tilt-hexarotor from tolerable faulty states accordingly. This work focuses on fast and computationally efficient allocation algorithms as it treats a real-time application capable of rapid movements. Promising results are achieved by the Cascading Moore-Penrose inverse (CMPI), which is an extension to the already implemented MPI. Nevertheless, some sources also mention disadvantages in the actuator rate performance and the behavior on actuator saturation[20][23][24][46]. Thus, this work aims at evaluating and possibly improving this method to achieve the desired performance. Another optimization algorithm based on the interior point method, which is unlikely to have been applied to a fully actuated UAV, is evaluated as an alternative solution to the control allocation problem. It considers the constraints through a cost function that allows for the consideration of other optimization criteria such as power efficiency. This thesis proposes the formulation of a quadratic program for this matter. Technically, this can be applied solely to linear models, and there exist methods to sequentially linearize the system and cost function for each time step [76]. This limitation is avoided here by using an input transformation, termed *extended thrust formulation*. In addition, emergency routines are designed to maintain the overall system stability even if the allocation algorithm fails to find an admissible solution. The reconfigurable control allocation approaches are tested and compared in terms of algorithm completeness, time consumption, and rotor failures. Moreover, the results of the algorithms used in closed-loop tests for trajectory tracking are provided as well.

**Task priority control** Exploiting the redundancy of the proposed aerial manipulator, a control law is designed to achieve the desired end-effector configuration and perform secondary tasks in order of priority during the mission. The primary motion control is based on exact linearization [4], while the control law of secondary objectives is inspired by the task priority control established for redundant manipulators [149]. By limiting the attention to aerial manipulation, which involves more challenging issues with respect to



ground manipulators, three secondary tasks are designed in the following order: a) collision avoidance, b) center of gravity alignment, c) preferred joint configuration. In contrast to [113], whereby the priority-based control is designed at the speed level, multi-tasks have been investigated at the acceleration level in this thesis. The entire trajectory, including acceleration, can be tracked at the expense of a more complex structure, and speed jumps are prevented. Thanks to the nested structure, more secondary tasks can be easily added without worrying about affecting the performance of higher-priority tasks.

## **1.5 Thesis Structure**

The thesis is organized as follows. Following this introduction, Chapter 2 describes the preliminaries of this research, including 3D rigid transformations, orientation representations, long short-term memory, and some mathematical fundamentals. Chapter 3 presents the design and modeling of the aerial manipulator, which serves as the basis for further work. Subsequently, two allocation algorithms are introduced for the aerial vehicle in Chapter 4, which are reconfigurable in case of a fault in the propulsion system. Furthermore, emergency routines are utilized for the situation in which the control allocation is not solvable. The performance of both algorithms is compared in terms of completeness, time consumption, and failure adaptability. Chapter 5 presents fault detection, isolation, and estimation design based on a well-trained artificial neural network. Then, the performance of this data-driven approach is discussed based on the results from Monte Carlo simulation. In Chapter 6, filter-based observers are developed to estimate forces and torques. It also details the timing statistics and the estimation accuracy with a case study. After introducing the interpolation method for SE(3) and the possible procedure to minimize the risk of input saturation in Chapter 7, Chapter 8 proves the differential flatness property of the aerial manipulator, which allows controller design with exact linearization. In addition, it describes the secondary tasks and the impedance filter with evaluation results by numerical simulation. Chapter 9 is devoted to integrating contributions introduced and tested in the previous chapters, starting with explaining the overall fault-tolerant control scheme and test results with failure injection in randomly selected propulsion units, followed by the performance evaluation of the hybrid task priority control. The results and achievements of this thesis are summarized in Chapter 10, including suggestions for the future.

